Effects of light intensity on reflective ghost imaging

Deyang Duan (段德洋)[1], Shaojiang Du (杜少将)[2], Li Yan (闫 丽)[3], Shengshan Jiang (姜盛山)[3], Yuanyuan Liu (刘元元)[3], Lu Zhang (张 路)[3], and Yunjie Xia (夏云杰)[1*]

[1]*Shandong Provincial Key Laboratory of Laser Polarization and Information Technology, Research Institute of Laser, Qufu Normal University, Qufu 273165, China*

[2]*School of Physics and Information Technology, Jining University, Qufu 273155, China*

[3]*School of Physical Engineering, Qufu Normal University, Qufu 273165, China*

[*]*Corresponding author: yjxia@mail.qfnu.edu.cn*

Received February 11, 2014; accepted April 20, 2014; posted online June 20, 2014

In this letter, we analyze the effects of light intensity on reflective ghost imaging with thermal source. We find that the brightness of reflective ghost image can be changed by modulating the light intensity of the source and the splitting ratio of the beam splitter. The signal-to-noise ratio will be improved by increasing the light intensity of the source. More important, we can obtain the reflective ghost image with high image quality by adopting a low light intensity signal beam and a high light intensity reference beam, which is better than the classical optical imaging, because it can reduce the effects of light on the object.

OCIS codes: 270.5290, 030.6600.
doi: 10.3788/COL201412.072701.

Ghost imaging is a procedure for forming the image of an object indirectly, by means of correlation between two light beams to image an object without spatially resolving measurements of the light beam that has undergone object interaction. Ghost imaging is so-called because the photons that provide the spatial information regarding the object have never directly interacted with the object to be imaged. Recent work[1] shows that the ghost imaging has significant meanings in understanding the quantum correlations. So the ghost imaging may be applied in the quantum information in the future.

An important reason of concerning about the ghost imaging over the last decade is its potential applications in many areas[2−11]. For example, biomedical imaging[9,11] and optical encryption[10]. In the previous works, many factors affecting the image quality of ghost imaging, such as the source[12,13], lens[14], and atmospheric turbulence[15−18], were theoretically and experimentally analyzed in transmission-type ghost imaging system[19−21]. Yet remote sensing[25,26] applications require that the objects can be imaged in reflection. Recently, many works have also demonstrated the feasibility of reflective ghost imaging[6,15,22−26]. In this letter, we analyze the effects of light intensity on reflective ghost imaging with thermal source in brightness, image contrast, and signal-to-noise ratio (SNR). Certainly, the transmission case can also be obtained based on our analysis.

We consider the reflective ghost imaging configuration in Fig.1. A laser beam passes through a rotating ground-glass (RG) to produce spatial incoherent signal and reference beams whose temporal bandwidths are much lower than those of the bucket detector and high spatial-resolution detector (charge-cuupled device (CCD) array). The signal beam interacts with the object, but the reference beam does not interact with the object. Cross correlating the currents from the two detectors yields the ghost image, whose physical origin lies in the perfect correlation between the spatial fluctuations imposed by the source plane on the signal and reference beams.

Two optical beams generated by a laser beam, a signal field $\hat{E}_{\rm S}(\boldsymbol{\rho},t)e^{-i\omega_0 t}$ and a reference field $\hat{E}_{\rm R}(\boldsymbol{\rho},t)e^{-i\omega_0 t}$, that are scalar, positive-frequency, paraxial field operators normalized to have units $\sqrt{\text{photons/m}^2\text{s}}$ units. The quantities ρ and ω_0 are the transverse coordinate and center frequency, respectively. The commutation relations for the base-band field operators are given by[27],

$$[\hat{E}_m(\boldsymbol{\rho}_1,t_1),\hat{E}_\ell(\boldsymbol{\rho}_2,t_2)]=0, \tag{1}$$

$$[\hat{E}_m(\boldsymbol{\rho}_1,t_1),\hat{E}^\dagger_\ell(\boldsymbol{\rho}_2,t_2)]=\delta_{m,\ell}\,\delta(\boldsymbol{\rho}_1-\boldsymbol{\rho}_2)\delta(t_1-t_2)\,, \tag{2}$$

where $m,l=1,2$, δ_{ml} is the Kronecker delta, and $\delta(\cdot)$ is the unit impulse.

The currents from the bucket detector and each pixel on the CCD are sent to a correlator with coincidence measurement, whose output for the CCD pixel located at transverse coordinate ρ_1 is given by

$$\hat{C}(\boldsymbol{\rho}_1)=\frac{1}{T_I}\int_{-T_I/2}^{T_I/2}\mathrm{d}t\,\hat{\imath}_1(t)\hat{\imath}_2(t)\,, \tag{3}$$

where T_I is the average time and we have suppressed an L/c time delay in $\hat{\imath}_1(t)$ that is need to account for the

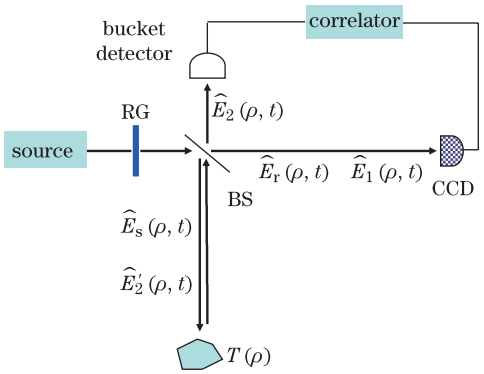

Fig. 1. Setup of the reflective ghost imaging.

delay incurred by the reflective light from the object.

indent We consider two ideal detectors that are assumed to have identical subunity quantum efficiencies and finite electrical bandwidths with no dark current or thermal noise contributing to the output current. The output currents corresponding to the following quantum measurements are given by[28,29]

$$\hat{i}_m(t) = q\int \mathrm{d}\tau \int_{\mathcal{A}_m} \mathrm{d}\boldsymbol{\rho}\, \hat{E}^{\dagger}_{\eta,m}(\boldsymbol{\rho},\tau)\hat{E}_{\eta,m}(\boldsymbol{\rho},\tau)h_B(t-\tau), \tag{4}$$

where $\mathcal{A}_1$ and $\mathcal{A}_2$ denote the area of one pixel in the reference arm and the photosensitive surface of the bucket detector; q is the electron charge; $h_B(t)$ is a real impulse response to model the real detector's finite electrical bandwidth.

$$\hat{E}_{\eta,m}(\rho,t) \equiv$$

$$\begin{cases} \sqrt{\eta}\,\hat{E}_m(\boldsymbol{\rho},t) + \sqrt{1-\eta}\,\hat{E}_{\mathrm{vac},m}(\boldsymbol{\rho},t), m=1 \\ \sqrt{\eta}\,T(\boldsymbol{\rho})\,\hat{E}_m(\boldsymbol{\rho},t) + \sqrt{1-\eta|T(\boldsymbol{\rho})|^2}\,\hat{E}_{\mathrm{vac},m}(\boldsymbol{\rho},t), m=2, \end{cases} \tag{5}$$

where $\sqrt{\eta}$ is the detector's quantum efficiency, and $\hat{E}_{\mathrm{vac},m}(\boldsymbol{\rho},t)$ is a Vacuum-state field operator. The function $\hat{E}_{\eta,1}(\rho,t)$ represents the reference light detected by the CCD array, and the function $\hat{E}_{\eta,2}(\rho,t)$ represents the light field detected by the bucket detector.

$$\hat{E}_1(\boldsymbol{\rho},t) = \int \mathrm{d}\rho' \hat{E}_r(\boldsymbol{\rho}',t)h_l(\rho'-\rho), \tag{6}$$

$$\hat{E}_2(\boldsymbol{\rho},t) = \int \mathrm{d}\rho' \hat{E}'_2(\boldsymbol{\rho}',t)h_l(\rho'-\rho)T(\rho'), \tag{7}$$

$$\hat{E}'_2(\boldsymbol{\rho}',t) = \int \mathrm{d}\rho'' \hat{E}_s(\boldsymbol{\rho}'',t)h_l(\rho''-\rho), \tag{8}$$

where $h_l(\rho)$ is the Huygens-Fresnel-Green's function:

$$h_l(\rho) = \frac{k_0 e^{ik_0(L+\frac{|\rho|^2}{2L})}}{2i\pi L}, \tag{9}$$

$k_0 = \omega_0/c$ is the wave number associated with the center frequency, $T(\rho)$ is the object's field-reflection coefficient. We have neglected time delays.

Because the objects for reflective ghost imaging will have microscopic surface variations–from a nominal, smooth surface profile—whose standard deviations can greatly exceed the illumination wavelength and whose transverse correlation scale can be sub-wavelength. If this object is illuminated by laser, it gives rise to laser speckle in the reflective signal beam. Therefore, we will use a reasonable statistical model for $T(\rho)$[6,30].

$$\langle T(\rho_1)T(\rho_2)\rangle = \lambda_0^2 \mathcal{T}(\boldsymbol{\rho}_1)\delta(\boldsymbol{\rho}_1-\boldsymbol{\rho}_2), \tag{10}$$

where λ_0 is the center wavelength of the illumination light, and we will omit it in the following calculation. $\mathcal{T}(\boldsymbol{\rho}_1)$ is physically the mean square speckle reflection coefficient at location ρ_1, and at the same time, it represents the object information that is sought.

The $\hat{C}(\boldsymbol{\rho}_1)$ measurement produces an unbiased estimate of the ensemble-average equal-time current cross-correlation function,

$$\begin{aligned}\langle \hat{C}(\rho_1)\rangle &= \langle \hat{i}_1(t)\hat{i}_2(t)\rangle = q^2\eta^2\mathcal{A}_1 \\ &\times \int_{\mathcal{A}_2} d\boldsymbol{\rho} \int du_1 \int du_2\, h_B(t-u_1)h_B(t-u_2) \\ &\times \langle \hat{E}_1^{\dagger}(\boldsymbol{\rho}_1,u_1)\hat{E}_2^{\dagger}(\boldsymbol{\rho},u_2)\hat{E}_1(\boldsymbol{\rho}_1,u_1)\hat{E}_2(\boldsymbol{\rho},u_2)\rangle . \end{aligned} \tag{11}$$

We have used the commutation relations (1) and (2) to put the integrand into normal order. Next, the Gaussian-state moment-factoring theorem is utilized to the fourth-order moment[13,22,31], replacing the fourth-order moment with expressions that depend only on the second-order moments of the light fields,

$$\begin{aligned}\langle \hat{C}(\rho_1)\rangle &= q^2\eta^2\mathcal{A}_1 \\ &\times \int_{\mathcal{A}_2} d\boldsymbol{\rho} \int du_1 \int du_2\, h_B(t-u_1)h_B(t-u_2)\mathcal{T}(\boldsymbol{\rho}_1) \\ &\times \Big(\langle \hat{E}_1^{\dagger}(\boldsymbol{\rho}_1,u_1)\hat{E}_1(\boldsymbol{\rho}_1,u_1)\rangle\langle \hat{E}_2^{\dagger}(\boldsymbol{\rho},u_2)\hat{E}_2(\boldsymbol{\rho},u_2)\rangle \\ &+ \left|\langle \hat{E}_1^{\dagger}(\boldsymbol{\rho}_1,u_1)\hat{E}_2(\boldsymbol{\rho},u_2)\rangle\right|^2\Big). \end{aligned} \tag{12}$$

For thermal light, the signal and reference fields have the maximum phase-insensitive cross correlation but no phase-sensitive cross correlation[12,13,22]. In far field[13,32], we obtain the maximum phase-insensitive correlation function. The auto-correlation of the two detectors is given by

$$\begin{aligned}&\langle \hat{E}_m^{\dagger}(\rho_m,t)\hat{E}_m(\rho_m,t)\rangle \\ &= \frac{2P_m}{\pi a_L^2} e^{-(|\boldsymbol{\rho}_m|^2+|\boldsymbol{\rho_m}|^2)/a_L^2 - |\boldsymbol{\rho_m}-\boldsymbol{\rho_m}|^2/2\rho_L^2}, \end{aligned} \tag{13}$$

where $m = 1, 2$. The cross-correlation is expressed as

$$\begin{aligned}&\langle \hat{E}_1^{\dagger}(\rho_1,t_1)\hat{E}_2(\rho_2,t_2)\rangle \\ &= \frac{2P_3}{\pi a_L^2} e^{-(|\boldsymbol{\rho}_1|^2+|\boldsymbol{\rho}_2|^2)/a_L^2 - |\boldsymbol{\rho}_2-\boldsymbol{\rho}_1|^2/2\rho_L^2}, \end{aligned} \tag{14}$$

where $P_n = \int_{R^2} \mathrm{d}\rho \langle \hat{E}_m^{\dagger}(\boldsymbol{\rho},t)\hat{E}_l(\boldsymbol{\rho},t)\rangle$ is the photon flux[6,32], $n = 1,2,3$ and $m,l = 1,2$. Substitute Eqs. (13) and (14) into Eq. (12). When the intensity radius a_L is much larger than the object's transverse extent, the entire object is uniformly illuminated on average. Thus, we obtain the final form for the ensemble averaged photocurrent cross correlation,

$$\begin{aligned}\langle \hat{C}(\rho_1)\rangle = C_0 + C(\rho_1) &= \frac{q^2\eta^2\mathcal{A}_1\mathcal{A}_2}{L^2}\frac{4P_1P_2}{(\pi a_L^2)^2}\int \mathrm{d}\rho_2 \mathcal{T}(\boldsymbol{\rho}_2) \\ &+ \frac{q^2\eta^2\mathcal{A}_1\mathcal{A}_2}{L^2}\left(\frac{2P_3}{\pi a_L^2}\right)^2 \int \mathrm{d}\rho_2 e^{-|\boldsymbol{\rho}-\boldsymbol{\rho}_1|^2/\rho_L^2}\mathcal{T}(\boldsymbol{\rho}_2). \end{aligned} \tag{15}$$

The ghost image term can be seen as the object's intensity-reflection coefficient $\mathcal{T}(\boldsymbol{\rho}_2)$ convolved with a Gaussian point spread function.

We assume that the light intensity of source is expressed as I_0, so we obtain the photon flux that appears in the former,

$$P_1 = \alpha I_0; P_2 = (1-\alpha)\alpha I_0; P_3 = \sqrt{\alpha^2(1-\alpha)}\, I_0, \quad (16)$$

where α is the splitting ratio of the beam splitter. Fortunately, $P_1P_2 = P_3^2$. Eq. (15) shows that the brightness of reflective ghost image depends on the photon flux. When the light intensity of the source is increased, the brightness of reflective ghost image increases correspondingly. It is surprised that the brightness of ghost image can be changed by modulating the splitting ratio of beam splitter. In this scheme of reflective ghost imaging, the brightness has the maximum value when $\alpha = 2/3$. Thus, a high brightness ghost image can be obtained by using a low light intensity signal beam and a high light intensity reference beam, which can reduce the effect of light on the object. For example, the object is an animal or other organism that are very sensitive to light, and we want to study these objects' behavior in the dark or low light environment. In these cases, the ghost imaging shows incomparable superiority.

The image contrast of ghost image is defined as [6]

$$\mathcal{C} = \frac{\max_{\mathcal{R}}[C(\boldsymbol{\rho}_1)] - \min_{\mathcal{R}}[C(\boldsymbol{\rho}_1)]}{C_0}. \quad (17)$$

For simplicity, we will also assume that ρ_L is small enough to resolve all features in the object's intensity-reflection coefficient. So that

$$\int \mathrm{d}\rho_2 e^{-|\boldsymbol{\rho}-\boldsymbol{\rho}_1|^2/2\rho_L^2}\mathcal{T}(\boldsymbol{\rho}_2) = \pi\rho_L^2\mathcal{T}(\boldsymbol{\rho}_1), \quad (18)$$

thus

$$\mathcal{C} = \frac{P_3^2}{P_1P_2}\frac{\pi\rho_L^2}{A_T} = \frac{\pi\rho_L^2}{A_T}, \quad (19)$$

where $A_T = \int \mathrm{d}\rho_2\mathcal{T}(\boldsymbol{\rho}_2)$ is the effective area of the object. $\mathcal{C}$= 1/number of on-object resolution cells[6]. Therefore, the image contrast of reflective ghost image is not affected by the light intensity. From Eq. (15), we can see that the ghost image and background increase with the light intensity. And the extent of the ghost image and background are the same because $P_1P_2 = P_3^2$. At the same time, when we modulate the light intensity of the signal and reference beams, the image contrast is not affected.

We will use the method that is given by Erkmen *et al*[6,12] to calculate the SNR of reflective ghost imaging. The background-free ghost image can be obtained by means of ac-coupling[12,33]. Thus, we obtain the reflective ghost image with background-free. Eq. (15) becomes

$$\langle\hat{C}(\rho_1)\rangle = \frac{q^2\eta^2\mathcal{A}_1\mathcal{A}_2}{L^2}\left(\frac{2P_3}{\pi a_L^2}\right)^2\int d\rho_2 e^{-|\boldsymbol{\rho}-\boldsymbol{\rho}_1|^2/\rho_L^2}\mathcal{T}(\boldsymbol{\rho}_2). \quad (20)$$

Indeed, the only difference between Eq. (20) and the corresponding result[6,22] for the reflective ghost imaging is the photon flux P_3.

The SNR of ghost imaging is defined as

$$\mathrm{SNR} \equiv \frac{\langle\hat{C}(\boldsymbol{\rho}_1)\rangle^2}{\langle\Delta\hat{C}^2(\boldsymbol{\rho}_1)\rangle}, \quad (21)$$

where $\Delta\hat{C}(\boldsymbol{\rho}) \equiv \hat{C}(\boldsymbol{\rho}) - \langle\hat{C}(\boldsymbol{\rho})\rangle$. we can obtain the expression of SNR,

$$\mathrm{SNR} = \left(\mathcal{T}^2(\boldsymbol{\rho}_1)T_I/T_0\right) / \left(\frac{A_T'}{\sqrt{2\pi}\rho_L^2} + \frac{\mathcal{T}^2(\boldsymbol{\rho}_1)T_I\Gamma a_0^2}{4\pi T_0\mathcal{A}_2} + \frac{\mathcal{T}(\boldsymbol{\rho}_1)L^2}{\eta\mathcal{I}\mathcal{A}_2} + \frac{4\pi\rho_L^2\mathcal{T}^2(\boldsymbol{\rho}_1)}{3\mathcal{A}_1\eta\mathcal{I}} + \frac{\sqrt{\pi}\Omega_B T_0\rho_L^2\mathcal{T}(\boldsymbol{\rho}_1)L^2}{16\sqrt{2}\mathcal{A}_1\mathcal{A}_2\eta^2\mathcal{I}^2}\right), \quad (22)$$

where, $\mathcal{I} \equiv P_3T_0\rho_L^2/a_L^2$, $A_T' = \int \mathrm{d}\rho_2\,|\mathcal{T}(\boldsymbol{\rho}_2)|^2$, $\Gamma = \pi\int_{|\upsilon|\leqslant 4\varepsilon}\mathrm{d}\upsilon e^{-|\upsilon|^2/2}O(\upsilon)$. $\upsilon = \rho_L k_0(\rho' - \rho'')$ is the difference coordinates, $\rho\prime$ and ρ'' are the coordinates at the bucket detector.

The ghost image comes from the intensity cross-correlation function. Therefore, the SNR of thermal ghost image depends on the light intensity of source. Moreover, the SNR also depends on the splitting ratio of the beam splitter because $P_3 = \sqrt{\alpha^2(1-\alpha)}\, I_0$. Fortunately, we can obtain a reflective ghost image with high image quality by adopting a low light intensity signal beam and a high light intensity reference beam achieved by changing the splitting ratio. Figure 2 shows that the SNR of ghost imaging will increase with the increase of the light intensity of source. The SNR is dramatically enhanced when the light intensity is not very strong. However, the enhancement of the SNR is not dramatically when the light intensity continues to increase. Therefore, a source with reasonable light intensity is necessary to obtain the ghost image with high SNR, which is very important for ghost imaging in practical application.

Moreover, we have also analyzed the case of ghost imaging with quantum source. We find that the quantum case is similar to the thermal case including the brightness, image contrast and SNR. The SNR will also increase with the increase of light intensity of quantum source because the relationship between the SNR of ghost imaging with thermal and quantum source and total correlations is a quasi-liner ratio[1]. Of course, both the SNR and total correlations are bounded at high illumination.

In conclusion, our research work shows that the brightness of reflective ghost image can be changed by modulating the light intensity of the source and the splitting

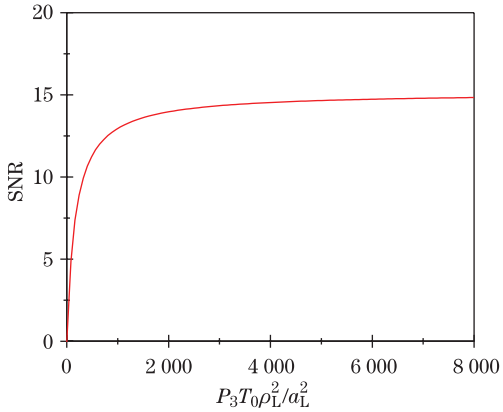

Fig. 2. Ghost imaging SNR plotted as the function of brightness, for $\mathcal{T}(\boldsymbol{\rho}_1) = 1$, $A_T'/\rho_L^2 = 10^3$, $\rho_L^2/\mathcal{A}_1 = 0.1$, $\eta = 0.9$, $T_I/T_0 = 10^4$, $a_0^2/\mathcal{A}_2 = 1/\pi$, $L^2/\mathcal{A}_2 = 10^5$, and $\Omega_B T_0 = 10$.

ratio of the beam splitter. The SNR depends on the light intensity of source, and can be changed by the splitting ratio. However, the image contrast of the reflective ghost image does no affected by the light intensity. More important, we find another advantage of ghost imaging compared with classical optical imaging, i.e., a ghost image with high brightness, high image contrast, and high SNR can be obtained by using a low light intensity signal beam and a high light intensity reference beam, which can reduce the effects of light on the object. This is very useful in biology.

This work was supported by the National Natural Science Foundation of China (Nos. 11204156, 61178012, 11304179, and 11247240). The Specialized Research Fund for the Doctoral Program of Higher Education (No. 20123705120002).

References

1. S. Ragy, G. Adesso, Sci. Rep. **2,** 651 (2012).
2. M. Li, Y. Zhang, K. Luo, L. Wu, and H. Fan, Phys. Rev. A **87,** 033813 (2013).
3. N. D. Hardy and J. H. Shapiro, Phys. Rev. A **87,** 023820 (2013).
4. F. Ferri, D. Magatti, L. A. Lugiato, and A. Gatti, Phys. Rev. Lett. **104,** 253603 (2010).
5. K. W. C. Chan, D. S. Simon, A. V. Sergienko, N. D. Hardy, J. H. Shapiro, Phys. Rev. A **84,** 043807 (2011).
6. H. D. Hardy, *Analyzing and Improving Image Quality in Reflective Ghost Imaging*, S.M. thesis (Massachusetts Institute of Technology, 2011).
7. D. Duan, and Y. Xia, J. Opt. Soc. Am. A **31,** 183-187 (2014).
8. Y. Li, H. Yang, J. Liu, L. Gong, Y. Sheng, W. Cheng, S. Zhao, Chin. Opt. Lett. **11,** 021104 (2013).
9. W. Gong and S. Han, Opt. Lett. **36,** 394-396 (2011).
10. P. Clemente, V. Durán, V. Torres-Company, E. Tajahuerce, and J. Lancis, Opt. Lett. **35,** 2391-2393 (2010).
11. M. Bina, D. Magatti, M. Molteni, A. Gatti, L. A. Lugiato, and F. Ferri, Phys. Rev. Lett. **110,** 083901 (2013).
12. B. I. Erkmen, J. H. Shapiro, Phys. Rev. A **79,** 023833 (2009).
13. B. I. Erkmen, J. H. Shapiro, Phys. Rev. A **77,** 043809 (2008).
14. D. S. Simon and A. V. Sergienko, Phys. Rev. A **82,** 023819 (2010).
15. N. D. Hardy and J. H. Shapiro, Phys. Rev. A **84,** 063824 (2011).
16. R. E. Meyers, K. S. Deacon, and Y. Shih, Appl. Phys. Lett. **98,** 111115 (2010).
17. J. Cheng, Opt. Express **17,** 7916 (2009).
18. K. W. C. Chan, D. S. Simon, A. V. Sergienko, N. D. Hardy, Phys. Rev. A **84,** 043807 (2011).
19. D. Duan. S. Du. L. Yan, S. Jiang, Y. Liu, L. Zhang, and Y. Xia, Eur. Phys. J. D **68,** 11 (2014).
20. D. Duan, S. Du, and Y. Xia, Phys. Rev. A **88,** 053842 (2013).
21. B. Cao, C. Zhang, and P. Ou, Chin. Opt. Lett. **9,** 081102 (2011).
22. D. Duan, Y. Xia, Chin. Opt. Lett, **10,** 031102 (2012).
23. C. Wang, D. Zhang, Y. Bai, and B. Chen, Phys. Rev. A **82,** 063814 (2010).
24. R. E. Meyers, K. S. Deacon, Y. H. Shih, J. Mod. Opt. **54,** 2381 (2007)
25. C. Zhao, W. Gong, M. Chen, E. Li, H. Wang, W. Xu, and S. Han, Appl. Phys. Lett. **101,** 141123 (2012).
26. W. Gong C. Zhao, J. Jiao, E. Li, arXiv:1301.5767.
27. H. P. Yuen and J. H. Shapiro, IEEE Trans. Inf. Theory **24,** 657 (1978).
28. H. P. Yuen and J. H. Shapiro, IEEE Trans. Inf. Theory **26,** 78 (1980).
29. J. H. Shapiro, Proc. SPIE **5111,** 382 (2003).
30. J. H. Shapiro,B. A. Capron, and R. C. Harney, Appl. Opt. **20,** 3292 (1981).
31. D. Duan, L. Zhang, and Y. Xia, J. Opt. Soc. Am. A **31,** 730 (2014).
32. B. I. Erkmen, J. H. Shapiro, Adv. Opt. Photon. **2,** 404 (2010).
33. H. Chen, T. Peng, and Y. Shih, Phys. Rev. A **88,** 023808 (2013).